Multi-Constraint Gerchberg-Saxton Iteration Algorithms for Linearizing IM/DD Transmission Systems

Hu, Shaohua; Zhang, Jing; Tang, Jianming; Jin, Taowei; Jin, Wei; Liu, Qun; Zhong, Zhuqiang; Giddings, Roger; Hong, Yanhua; Xu, Bo; Yi, Xingwen; Qiu, Kun

Optics Express

DOI:
https://doi.org/10.1364/OE.448826

Published: 14/03/2022

Peer reviewed version

Multi-Constraint Gerchberg-Saxton Iteration Algorithms for Linearizing IM/DD Transmission Systems

SHAOHUA HU,[1] JING ZHANG,[1,*] JIANMING TANG,[2] TAOWEI JIN[1], WEI JIN[2], QUN LIU,[1] ZHUQIANG ZHONG[2], ROGER GIDDINGS,[2] YANHUA HONG[2], BO XU,[1] XINGWEN YI[3], AND KUN QIU [1]

[1]*The Key Laboratory of Optical Fiber Sensing and Communications (Education Ministry of China), School of Communication and Information Engineering, University of Electronic Science and Technology of China, Chengdu, Sichuan 611731, China*
[2]*School of Electronic Engineering, Bangor University, Bangor, LL57 1UT, UK*
[3] *School of Electronics and Information Technology, Sun Yat-Sen University, Guangzhou 510275, China*
** zhangjing1983@uestc.edu.cn*

Abstract: Chromatic dispersion-enhanced signal-signal beating interference (SSBI) considerably affects the performance of intensity-modulation and direct-detection (IM/DD) fiber transmission systems. For recovering optical fields from received double sideband signals after propagating through IM/DD transmission systems, Gerchberg-Saxton (G-S) iterative algorithms are promising, which, however, suffers slow convergence speeds and local optimization problems. In this paper, we propose a multi-constraint iterative algorithm (MCIA) to extend the Gerchberg-Saxton-based linearized detection. The proposed technique can accelerate the convergence speed and realize nonlinear-equalization-free detection. Based on the data-aided iterative algorithm (DIA) and the decision-directed data-aided iterative algorithm (DD-DIA), the proposed technique reuses redundant bits from channel coding to not only correct decision errors but also enforce the constraints on the task function to further accelerate the whole optical field retrieval processing. Simulation results show that, compared with the DD-DIA, the MCIA reduces the received optical power (ROP) by about 1.5-dB for a 100-Gb/s over 50-km SSMF PAM-4 signal transmission at the SER of 2×10^{-2}. For a 100-Gb/s over 400-km SSMF transmission system, just 30 MCIA iterations is needed, which is 30% reduction in iteration count compared with the DD-DIA. For further increased transmission capacities, the MCIA can improve the symbol error rate (SER) by two orders of magnitude compared with the conventional IA. To validate the effectiveness of the MCIA, we also conduct experiments to transmit 92-Gb/s PAM-4 signals over 50-km IM/DD fibre systems. We find that the MCIA has an 1-dB ROP improvement compared with the DD-DIA. Compared with Volterra nonlinear equalization, the BERs of the MCIA with a simple linear equalizer are reduced by more than one order of magnitude with only 52 MCIA iterations.

1. Introduction

Intensity modulation and direct detection (IM/DD) transmission systems are widely deployed in short-reach and intra-data center interconnects because of their low system complexity and high cost-effectiveness. Signal-signal beating interference (SSBI) resulting from the interaction between fiber chromatic dispersion (CD) and square-law detection significantly limit their practically achievable signal transmission capacity versus reach performances[1]. Generally speaking, increasing signal bandwidths and/or transmission distances enhances the SSBI effect experienced by optical signals propagating through the IM/DD transmission systems. Owing to the SSBI's nonlinear nature, it is impossible to effectively compensate for the effect utilizing simple linear techniques developed for coherent detection systems [2]. To reduce the SSBI

effect, various technical solutions have been proposed, which can be classified into three categories: lite-coherent optical system design, physical SSBI mitigation and digital signal processing (DSP). The lite coherent optical system design is to recover complex-valued optical field signals using approaches including carrier assisted differential detection [3], same laser source-based self-homodyne detection [4] and Stokes vector reception [5]. The physical SSBI mitigation techniques of the second category utilize dual-drive Mach-Zehnder modulators (DD-MZM) [6], delay interferometers [7], fiber Bragg gratings(FBG) or dispersion compensation fibers [8] to manipulate the data-bearing optical fields to alleviate the SSBI effect. The techniques of these two categories are effective in mitigating the SSBI effect, but significant modifications must be made to the already installed IM/DD transmission links. Whilst the DSP techniques of the third category do not require any modifications to the existing IM/DD transmission systems, as they manipulate the signals in the digital domain by using approaches including, for example, precoding [9, 10], nonlinear equalization[11] and model-based iteration [12]. However, these DSP techniques are just capable of partially compensating for the SSBI effect, their supported signal transmission capacity versus reach performances are limited.

Recently, a Gerchberg-Saxton (G-S) iterative DSP technique, which is originated from optical imaging, has demonstrated potential for recovering optical fields in IM/DD transmission systems [13]. The G-S algorithm retrieves a complex-valued optical field in an iterative manner by utilizing multiple real-valued intensity image planes, thus enabling the linear reception of optical signals transmitted over the IM/DD transmission systems [14]. To implement the G-S algorithm in the IM/DD transmission systems, additional dispersive devices have been introduced to construct the multiple real-valued 1-D image planes.

From the practical application point of view, a DSP technique that requires neither modifications to the existing physical IM/DD system structures nor high receiver DSP complexity are highly preferable. For a representative IM/DD transmission system, there are two planes, i.e., the transmitter-side phase-intensity relationship and the receiver-side detected optical intensity. As a result, due to the poor global optimization performance [15], the conventional G-S algorithm fails to recover intensity-modulated signals when their data rates and transmission distances are above certain values. Although the G-S pre-compensation algorithms [16] can be used to compensate for channel distortions, the use of post-compensation in the G-S algorithm is, however, much easier in terms of applying more constraints to both the transmission systems and signals in order to achieve the desired global optimization performance of the algorithm. As a direct result, we have proposed a data-aided iterative algorithm (DIA) and its accelerated version termed decision-directed DIA (DD-DIA) to solve the local optimization problem of the G-S algorithm [17]. Our numerical simulations have shown that both the DIA and the DD-DIA can significantly improve the IM/DD transmission system performances, which are, however, still limited by the SSBI effect for higher data rates and/or long fiber lengths. In addition, a relatively large number of iterations are also needed to alleviate the local optimization problem.

In this paper, we propose a multi-constraint iterative algorithm (MCIA) to address the global optimization problem. The MCIA not only considers pilot symbols and decided symbols but also reuses redundant bits from channel coding to further accelerate the iteration convergence progress. Both numerical simulations and experimental measurements are undertaken. Our numerical simulations show that the MCIA improves the received optical power (ROP) by about 1.5-dB compared with the DD-DIA for a 100-Gb/s over 50-km SSMF system subject to an optical signal-to-power ratio (OSNR) of 37 dB. For a 100-Gb/s over 400-km SSMF transmission system, just 30 MCIA iterations are needed, this leads to a 30% reduction of the iteration count compared to the DD-DIA. The MCIA can also provide good compensation for large accumulated chromatic dispersions, this is evidenced by the fact that, compared with the conventional IA, the MCIA can improve the symbol error rate (SER) by two orders of magnitude for both 150-Gb/s over 500-km and 200-Gb/s over 300-km SSMF

transmission systems. Experimental demonstrations of 92-Gb/s PAM-4 over 50-km SSMF IM/DD transmissions based on the MCIA are reported and 1-dB ROP improvements compared to the DD-DIA are observed. Our results also show that the MCIA outperforms the Volterra nonlinear equalization: compared with the Volterra nonlinear equalization, for the considered transmission systems, the BERs are reduced by more than one order of magnitude with only 52 MCIA iterations.

This paper is organized as follows. In Section 2, we describe the principle of the proposed MCIA technique. In Section 3, we explore the MCIA's effectiveness in improving chromatic dispersion compensation capability, noise tolerance, receiver sensitivity and convergence speed. In Section 4, the performance improvement of the MCIA is experimentally verified with a C-band 92-Gbit/s PAM-4 over 50-km SSMF IM/DD transmission systems.

2. Principles of the MCIA

The signal recovery of the MCIA can be regarded as an optimization problem, where the objective is to reconstruct an optical field that minimizes the mean square error between the detected optical current $I_o(m)$ and the intensity of the reconstructed optical field $R_1(m)$. The task function can be expressed in Eq. (1),

$$\min \quad e(R_1) = \mathbf{E}\left[\left|\left\|R_1(m)\right\|^2 - I_o(m)\right|^2\right] \tag{1}$$

Clearly Eq.(1) belongs to a non-convex optimization problem due to the complicated nature of $I_o(m)$, thus the existence of insufficient constraints cannot enable the task function to achieve its ultimate goal of quickly realizing lowest BERs. To address such a challenge, three constraints can be introduced into Eq. (1), which are detailed below:

The first constraint is to introduce pilot symbols into the optical field reconstruction process in the receiver. By periodically inserting pilot symbols to the detected symbol sequence, we can primarily accelerate the convergence performance of the G-S algorithm. This is the process which has already been reported in the DIA algorithm. The second constraint is to use the decision process. As already described in the published DD-DIA algorithm, for each decision-directed iteration, a random selection of the decided symbols with a specific percentage is undertaken, and for the selected symbols, their continuously distributed amplitude values are replaced with the relevant target ones. The third constraint is to re-utilize the time-dependence of the binary bit sequence from channel encoding which is contained in the mapped symbol sequence. We can reuse the redundancy of forward error correction (FEC) to correct the decision errors in the DD-DIA immediately after the decision process.

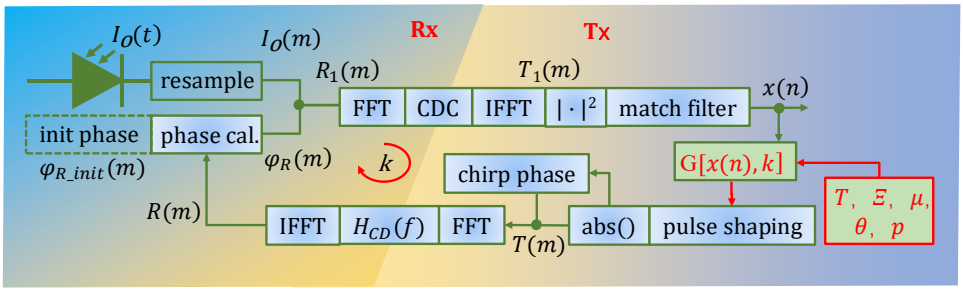

Fig. 1 The workflow of data-aided iterative algorithm for signal reconstruction.

For the MCIA, very similar to those associated with the conventional equalization process, the role of the pilot symbols introduced in the MCIA is to minimize the mean square error of the equalized symbols from the practically transmitted symbols. The second constraint related to the decision process is similar to the conventional equalizer with traceability such as DD-

LMS equalizer. But the major difference is that the decided symbols are randomly selected to avoid the local optimization problem. The decision and decoding operations generate pseudo-pilots of higher accuracy, which increase the density of pilot information but without affecting the overheads of physically transmitted signals. Therefore, all these constraints apply sufficient limitations to the task function, thus the optical field retrieval is improved.

Figure 1 depicts the DSP flowchart of the MCIA. If we define $x(n)$ as the down-sampled symbol sequence, $d_{pilot}(n)$ as the pilot symbols inserted before fiber transmissions in the digital domain, T and Ξ as the operators of the FEC and the maximum likelihood decision, then the pseudo-pilot signal can be selected from

$$x'(n) = \mathrm{T}\{\Xi[x(n)]\}, \tag{2}$$

and the signal transformation of the MCIA can be expressed as

$$\mathrm{G}[x(n),k] = \mu_{M,L}(n,k)d_{pilot}(n) + [1-\mu_{M,L}(n,k)]\left\{\theta(n,k)x'(n) + \left[1-\theta(n,k)\right]x(n)\right\}, \tag{3}$$

where $\mu_{M,L}(n,k)$ represents the training symbols allocation strategy at the n-th symbol and the k-th iteration, which has the following form

$$\mu_{M,L}(n,k) = \begin{cases} 1, & for\ \mathrm{mod}(n,M)=0\ \&\ \mathrm{mod}(k,L)<l \\ 0, & otherwise \end{cases}, l \in (0,L]. \tag{4}$$

The parameter M and L are the time and iteration interval of the pilot distribution [17]. $\theta(n,k)$ is a random signal that follows the Bernoulli distribution at the n-th symbol and the k-th iteration, which has

$$\Pr\{\theta=1\} = p,\ \Pr\{\theta=0\} = 1-p,\ p \in [0,1]. \tag{5}$$

Equations (2-5) are the general multi-constraint model of the MCIA. For the conventional G-S iterative algorithm, we have

$$\mu_{M,L}(n,k)=0,\quad \theta(n,k)=0, \tag{6}$$

and

$$\mathrm{G}[x(n),k] = x(n). \tag{7}$$

For the DIA, we have

$$\mu_{M,L}(n,k) \neq 0,\quad \theta(n,k)=0, \tag{8}$$

and

$$\mathrm{G}[x(n),k] = \mu_{M,L}(n,k)d_{pilot}(n). \tag{9}$$

For the DD-DIA, we have

$$\mu_{M,L}(n,k) \neq 0,\quad \theta(n,k) \neq 0,\quad T = I, \tag{10}$$

and

$$\mathrm{G}[x(n),k] = \mu_{M,L}(n,k)d_{pilot}(n) + [1-\mu_{M,L}(n,k)]\left\{\theta(n,k)\Xi(n) + \left[1-\theta(n,k)\right]x(n)\right\}, \tag{11}$$

where I is the identity operator, $I(a)=a$.

As illustrated in Fig.1, to implement the algorithms in the receiver, we firstly resample the PIN-detected signal by 2 samples per symbol. The initial phase $\varphi_{R\_init}(m)$ can be a linear function or an all-zero function over time, which is then multiplied by the detected optical current $I_o(m)$ to form a received signal $R_1(m) = \sqrt{A+I_o(mT_S)}\exp[\mathrm{j}\varphi_R(m)]$, where A is the bias of the intensity modulator, and T_S is the sampling period. Consequently, we apply frequency-domain inverse CD compensation to $R_1(m)$ and the transmitter-side-equivalent optical field $T_1(m)$ can be expressed by

$$T_1(f) = R_1(f)H_{CD}(f) = E_{Tx}(f)\mathrm{e}^{j\pi D\frac{\lambda^2}{c}Lf^2}, \tag{12}$$

where D, λ, c, L, and f represent the fiber dispersion, the central wavelength, the velocity of light, the transmission distance and the frequency variable, respectively. After match filtering and down-sampling, we have the symbol sequence $x(n)$. Then, the pilot and pseudo-pilot symbol insertions are applied corresponding to Eq. (3).

After up-sampling and pulse shaping of the symbols obtained after the abovementioned digital operations, intensity modulation is then performed to convert the symbols from the electrical domain to the optical domain, the phase of the optical field is produced according to the specific chirp phase model described in [18]. The output optical field $T(m)$ is then digitally forward-propagated through the fiber, after that the initial signal phase $\varphi_{R\_init}(m)$ is replaced with $\varphi_R(m) = \measuredangle F^{-1}\{F[T(m)]H_{CD}(f)\}$, an updated version of the receiver-side-equivalent optical field is formed. Thus, an entire cycle of the MCIA iteration is completed. By appropriately selecting the parameters in Eq. (3), we can have a variety of combinations that can optimize the signal recovery performance.

3. Simulation and discussions

To investigate the effectiveness of the MCIA in compensating for the accumulated transmission system CD effect, numerical simulations are first conducted using VPI. Here double sideband (DSB) PAM-4 IMDD optical transmission systems are considered. At the transmitter, a pseudo random bit sequence is first loaded and subsequently encoded by the Hamming linear block code, which is then mapped onto PAM-4 levels. A random PAM-4 pilot symbol is inserted into every *M* PAM-4 modulated symbols. Following an up-sampling operation at a factor of 2, a square-root raised cosine (SRRC) filter with a roll-off factor of 0.1 is applied to the symbol sequence to improve the spectral efficiency and partially eliminate CD-induced signal distortions. Electrical-to-optical (E/O) conversion is realized by a Mach-Zehnder modulator (MZM) biased at Vπ/4=2.5V, where an input continuous optical waveform operates at a wavelength of 1550 nm and has a linewidth of 100 kHz. The driving amplitude of the MZM is 0.4 V to ensure that the MZM modulator operates at its linear region. The modulated optical signal emerging from the MZM is transmitted, at an optical launch power of -2 dBm, through the SSMFs of different lengths. The SSMF parameters are: an attenuation coefficient of 0.2 dB/km and a dispersion parameter of 16 ps/(nm·km). After the fiber transmission, AWGN is loaded to the optical signal. An EDFA is introduced to adjust the received optical power (ROP) by a PIN photodiode with a thermal noise of 10×10^{-12} A/Hz$^{1/2}$ and a responsivity of 1A/W.

For two transmission systems including 150-Gb/s over 500-km SSMFs and 200-Gb/s over 300-km SSMFs, their numerically simulated SERs versus OSNR performances are plotted in Fig.2 for the MCIA, the DD-DIA, the DIA, the conventional IA and the Volterra nonlinear equalization with parameters having an acceptable computational complexity. In performing the MCIA and the DD-DIA, 50 DIA iterations are first implemented for pre-convergence, which are then followed by 50 MCIA or DD-DIA iterations. The DIA alone case has 100 iterations in total with an overhead of 10%. The conventional IA is the G-S based iterative algorithm also with 100 iterations in total. In all of these four algorithms, phase re-initializations are not introduced because the random initializations may result in sharp rises of SERs and also increase the total number of iterations required. As a reference, performance comparisons are also made between these four algorithms and a 3-order Volterra filter (VF), whose taps are taken to be 100, 11 and 5. It is shown in Fig.2 that for all these considered transmission systems, the large accumulated fiber CDs result in a complete failure of VF because the equalization model is under-fitted. In addition, neither the conventional IA and nor the 10% DIA can also recover the signal because of the local optimization problem. In sharp contrast, the DD-DIA and the MCIA have a significantly improved capability of dealing with the global optimization problems, as a direct result, compared with the DIA, the MCIA (DD-DIA) has two (one) order of magnitude SER improvement, as shown in Fig.2. By comparing Fig.2(a) and Fig.2(b), it is also seen that the aforementioned SER improvements still remain

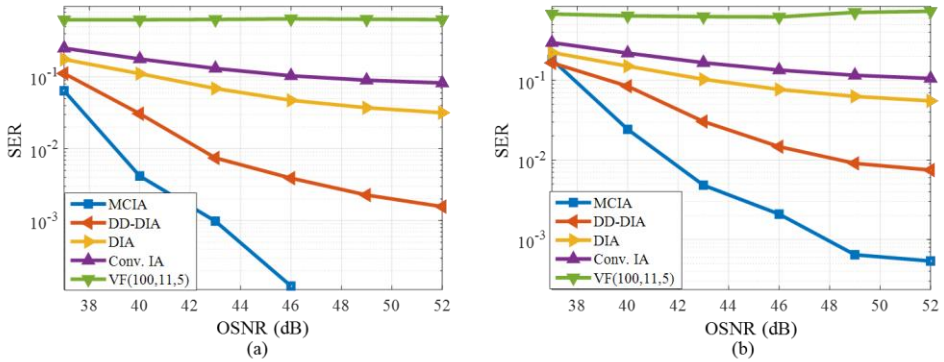

Fig. 2 Noise tolerance improvement of MCIA compared with existing algorithms. The ROP is -8 dBm. (a) 150 Gb/s@500 km; (b) 200 Gb/s@300 km.

when increasing the data rates from 150 Gb/s to 200 Gb/s. The large slopes of the OSNR-dependent SER curves indicate the MCIA's strong dispersion compensation capability.

To explore the receiver sensitivity of the MCIA, a 100-Gb/s PAM-4 DSB optical signal is transmitted over 50-km SSMFs at an OSNR of 37-dB. In Fig. 3, we show SERs versus ROP for different algorithms considered in this paper. The VF still cannot recover the signal and the IA and DIA also fail to produce acceptable SERs. The main reason behind the failure of the VF, conventional IA and DIA is because of the channel-equalizer model mismatch and the local optimization problem under such non-convex optimization conditions. On the other hand, both the DD-DIA and the MCIA can successfully recover the received data at relatively low ROPs. For example, the required ROP of the MCIA is -13 dBm at the SER of 2×10^{-2}, which gives rise to an 1.5-dB power budget improvement compared with the DD-DIA. For both the DD-DAI and the MCIA, their error floors are because of residual fiber dispersion and channel noise.

In order to explore the influence of the constraints on the algorithm convergence performance when the constraints are applied to them, here we randomly select 6 symbols and depict their amplitudes as a function of iteration index, as shown in Fig. 4. In Fig.4(b) and Fig.4(c), only the DIA is introduced in the first 80 iterations for pre-convergence, immediately following which the DD-DIA and the MCIA are then deployed from the 81-th iteration. In the numerical simulations, 100-Gb/s over 400-km SSMF DSB PAM-4 transmission systems are considered and their corresponding OSNRs and ROPs are fixed at 37 dB and -4dBm, respectively. In Fig. 4(a), the amplitudes obtained using the DIA are just partially converged with visible deviations from their target values. In Fig. 4(b), the utilization of the DD-DIA almost eliminates the amplitude deviations, however, rapid amplitude fluctuations still occur, which are caused by the random amplitude correction operation after the decision process, and the variance of the amplitude fluctuation is a direct result of decision errors. The decision errors do not affect the overall DD-DIA performance considerably as the majority of the decided symbols can still ensure the convergence of the algorithm. In Fig. 4(c), the decoder in the MCIA corrects most of the aforementioned decision errors, thus giving rise to significantly reduced variances of the amplitude fluctuation curves and also accelerated amplitude convergence processes, as shown in Fig.4(c).

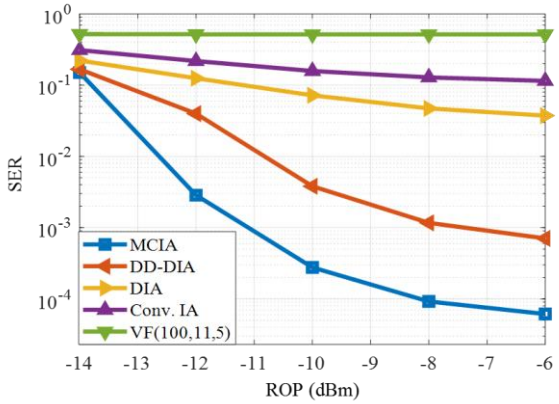

Fig. 3 PD sensitivity tolerance improvement of the MCIA compared with existing algorithms. 100 Gb/s 50 km @ 37dB OSNR.

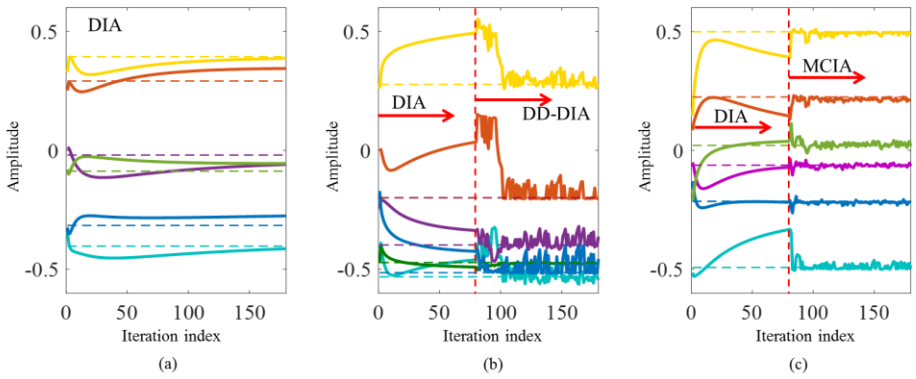

Fig. 4 The signal amplitude convergence curve of six random time slots varying along the iteration. The dashed lines are the target amplitudes. The solid lines are the calculated value.

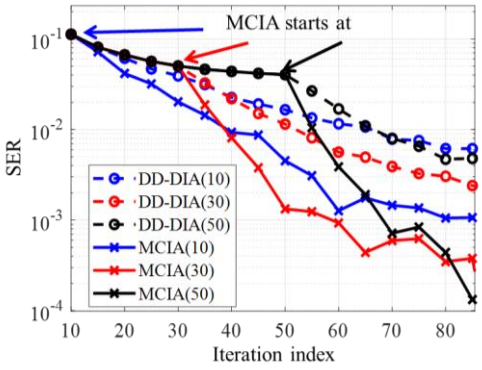

Fig. 5 The convergence curve of the DD-DIA and the MCIA enable from different starting points. 100 Gb/s 400km transmission at the ROP of -8 dBm and the OSNR of 40 dB.

Fig.4 suggests that for both the DD-DIA and the MCIA, an appropriate selection of the DIA-based pre-convergence iteration cycles may not only accelerate the convergence progresses but also reduce the SERs. This statement is verified in Fig.5, where SERs of the

DD-DIA and the MCIA are plotted as a function of iteration index for three different cases where the DD-DIA and the MCIA start at the DIA-based iteration cycles of 10, 30, and 50. As expected from Fig.4, Fig. 5 shows that the MCIA reduces the SERs more rapidly than the DD-DIA. When the total number of iterations is large enough, all the SER curves of the MCIA are approximately one order of magnitude lower than the DD-DIA. The minimum required number of iterations for the MCIA for reaching a SER of 2×10^{-2} can be as low as about 30, which are just half of the iteration cycles required by the DD-DIA.

The above results show that the MCIA can make full use of the advantages associated with the G-S field retrieval, decision-directed linear equalization and encoding redundancy to linearize the IMDD transmission systems by effectively reducing the SSBI effect. In addition, compared with the previous work, the MCIA has the fastest convergence speed.

4. Experiment demonstrations

In this section, we conduct experiments to transmit 92-Gb/s PAM-4 DSB optical signals over 50-km SSMFs to experimentally verify the data recovery performance of the MCIA. The experimental setup is illustrated in Fig. 6(a). An encoded PAM-4 waveform is loaded to an 8-bit DAC operating at 92 GSa/s. The signal emerging from the DAC passes through a radio frequency amplifier (RFA) and is then modulated onto a 1550-nm wavelength using an MZM with a bandwidth of 35 GHz. An external cavity laser with a linewidth of ~150 kHz and an output optical power of 10 dBm is utilized as an input to the MZM. The MZM-modulated optical signal is transmitted over 50-km G.652 SSMFs with an optical launch power of 2 dBm. After fiber transmissions, an EDFA with a noise figure of 5 dB is introduced to compensate for the fiber loss. A variable optical attenuator (VOA) is then introduced to adjust the optical power received by a TIA-free single-ended PD with a bandwidth of 40-GHz. The detected optical current is sampled by a 59-GHz digital phosphor oscilloscope (DPO) at 200 GSa/s. The transceiver DSP flowchart is illustrated in Fig. 6(b) and (c). To further maximize the transmission performance, as shown in Fig.6(c), a 20-tap FFE is used for pre-distortion to compensate for the bandwidth limitation, and the FFE coefficients are calculated for a back to back (B2B) case. Note that for both the DD-DIA and the MCIA, their constraints are not applied in every iteration. We alternate the iteration count for the pre-convergence IA and the start iteration cycles for both the DD-DIA and the MCIA, in order to achieve, for individual algorithms, optimum trade-offs between global optimization improvement and computational complexity. After the DD-DIA and the MCIA, an FFE is used to compensate for residual signal distortions induced by channel imperfections.

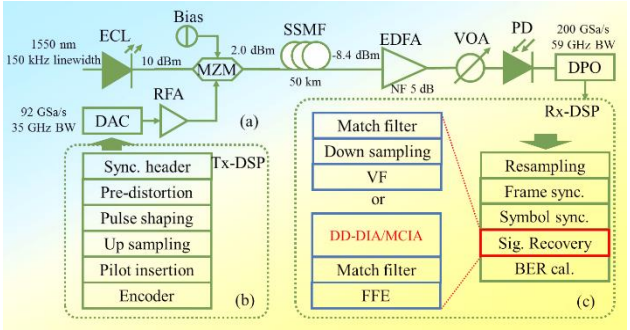

Fig. 6 Experimental setup and DSP flowchart of the transceiver. ECL, external cavity laser; RFA, radio frequency amplifier; VOA, variable optical attenuator; DPO, digital phosphor oscilloscope; VF, Volterra filter; FFE, forward feed equalizer.

The measured BERs versus ROP for both the DD-DIA and the MCIA are shown in Fig.7(a), where the corresponding results obtained using Volterra equalization VF (200, 11,7) are also plotted. It is shown in Fig.7(a) that the VF completely fails in recovering the signal over the entire ROP variation range considered here, while the DD-DIA and the MCIA can reduce the BERs to values well below 2×10^{-2}. More importantly, the BER curves for both the DD-DIA and the MCIA show no signs of developing any error floors, indicating that most of the SSBI-induced signal distortions are compensated and the channel noise is a dominant factor limiting the transmission system's BER performances. In addition, compared with the DD-DIA, the MCIA has an about 1 dB receiver sensitivity improvement. Moreover, it is also found that the MCIA+FFE31 and the MCIA+FFE150 have very similar BER performances, this indicates that the MCIA allows a simpler equalizer to be used. Fig.7 (b) and Fig. 7(c) depict the spectra and corresponding eye diagrams before and after the implementation of the MCIA at the ROP of 10 dBm, respectively. By comparing these two figures, it can be easily seen that the MCIA is capable of compensating for all of the frequency selective power fading-induced spectral nulls as deep as >25-dB, as a direct result, the open eye-diagrams are observed after the MCIA. The experimental convergence curve of the MCIA is presented in Fig.8, where the BER is reduced from 7×10^{-2} to 3.8×10^{-3} with a total number of iterations (the MCIA and conventional G-S) of 180, within which only 52 MCIA iterations are utilized. The measured experimental results indicate that the combination of the MCIA and the conventional G-S algorithm can reduce both the BERs and the DSP complexity.

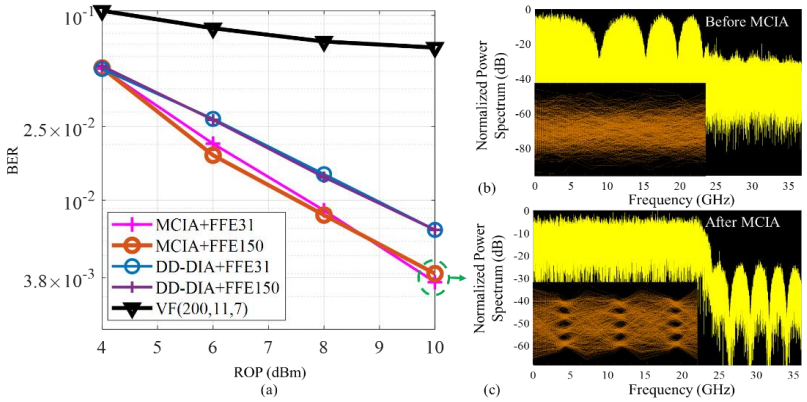

Fig. 7 Signal recovery performance comparison with the experimentally captured 92 Gb/s PAM-4 signal transmitted over 50-km SSMF. (b) and (c) are the electrical spectra and eye-diagrams before and after the MCIA.

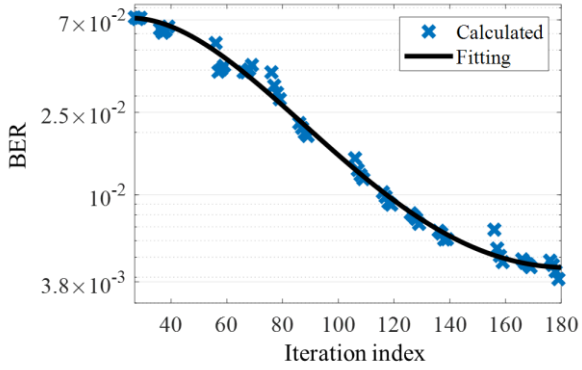

Fig. 8 Experimental convergence curve of the MCIA at the ROP of 10 dBm.

5. Conclusion

We have presented and experimentally demonstrated the proposed MCIA based on the G-S interactive algorithm for optical field recovery in the IM/DD PAM-4 signal transmission systems. The MCIA further accelerates the converge process compared to the DD-DIA, and improve the transmission performance compared to Volterra equalization. Combined with linear equalization, the MCIA can achieve more than one order of magnitude BER reduction compared with Volterra nonlinear equalization. The required iterations of the MCIA is significantly decreased compared with the DD-DIA.

Acknowledgement

National Science Foundation of China (NSFC) (61871082 and 62111530150), the state Key Laboratory of Advanced Optical Communication Systems and Networks, Shanghai Jiao Tong University (2020GZKF014), Fundamental Research Funds for the Central Universities (ZYGX2020ZB043 and ZYGX2019J008), Open Fund of IPOC (BUPT) (No. IPOC2020A011) and the program of China Scholarships Council (No. 201906070011)

References

1. Z. Li, M. S. Erkilinc, K. Shi, E. Sillekens, L. Galdino, B. C. Thomsen, P. Bayvel, and R. I. Killey, "SSBI Mitigation and the KramersPIP,вЂ‰Kronig Scheme in Single-Sideband Direct-Detection Transmission With Receiver-Based Electronic Dispersion Compensation," J. Lightwave Technol. **35**, 1887-1893 (2017).
2. K. Kikuchi, "Fundamentals of Coherent Optical Fiber Communications," J. Lightwave Technol. **34**, 157-179 (2016).
3. W. Shieh, C. Sun, and H. Ji, "Carrier-assisted differential detection," Light Sci Appl **9**, 18-18 (2020).
4. Y. J. Wen, A. Li, Q. Guo, Y. Cui, and Y. Bai, "200G self-homodyne detection with 64QAM by endless optical polarization demultiplexing," Opt. Express **28**, 21940-21955 (2020).
5. D. Che, C. Sun, and W. Shieh, "Optical Field Recovery in Stokes Space," J. Lightwave Technol. **37**, 451-460 (2019).
6. X. Ruan, L. Zhang, F. Yang, Y. Zhu, Y. Li, and F. Zhang, "Beyond 100G Single Sideband PAM-4 Transmission With Silicon Dual-Drive MZM," IEEE Photon. Technol. Lett. **31**, 509-512 (2019).
7. X. Li, S. Zhou, H. Ji, M. Luo, Q. Yang, L. Yi, R. Hu, C. Li, S. Fu, A. Alphones, W. Zhong, and C. Yu, "Transmission of 4×28-Gb/s PAM-4 over 160-km single mode fiber using 10G-class DML and photodiode," in *2016 Optical Fiber Communications Conference and Exhibition (OFC)*, 2016), 1-3.
8. T. F. Hussein, M. R. M. Rizk, and M. H. Aly, "A hybrid DCF/FBG scheme for dispersion compensation over a 300 km SMF," Opt. Quantum Electron. **51**, 1-16 (2019).
9. M. Xiang, Z. Xing, X. Li, E. El-Fiky, M. Morsy-Osman, Q. Zhuge, and D. V. Plant, "Experimental study of performance enhanced IM/DD transmissions combining 4D Trellis coded modulation with precoding," Opt Express **26**, 32522-32531 (2018).
10. Z. Xing, M. Xiang, E. El-Fiky, X. Li, M. G. Saber, L. Xu, P.-C. Koh, and D. V. Plant, "Experimental Demonstration of 600 Gb/s Net Rate PAM4 Transmissions Over 2 km and 10 km With a 4-PħB» CWDM TOSA," J. Lightwave Technol. **38**, 2968-2975 (2020).
11. H. Wang, J. Zhou, D. Guo, Y. Feng, W. Liu, C. Yu, and Z. Li, "Adaptive Channel-Matched Detection for C-Band 64-Gbit/s Optical OOK System Over 100-km Dispersion-Uncompensated Link," J. Lightwave Technol. **38**, 5048-5055 (2020).
12. Z. Li, M. S. Erkılınç, S. Pachnicke, H. Griesser, R. Bouziane, B. C. Thomsen, P. Bayvel, and R. I. Killey, "Signal-signal beat interference cancellation in spectrally-efficient WDM direct-detection Nyquist-pulse-shaped 16-QAM subcarrier modulation," Opt Express **23**, 23694-23709 (2015).
13. G. Goeger, C. Prodaniuc, Y. Ye, and Q. Zhang, "Transmission of intensity modulation-direct detection signals far beyond the dispersion limit enabled by phase-retrieval," in *2015 European Conference on Optical Communication (ECOC)*, 2015, 1-3.
14. H. Chen, N. K. Fontaine, J. M. Gene, R. Ryf, D. T. Neilson, and G. Raybon, "Dual Polarization Full-Field Signal Waveform Reconstruction Using Intensity Only Measurements for Coherent Communications," J. Lightwave Technol. **38**, 2587-2597 (2020).
15. H. H. Bauschke, P. L. Combettes, and D. R. Luke, "On the structure of some phase retrieval algorithms," in *International Conference on Image Processing* (IEEE, 2002), pp. II-II, doi: 10.1109/ICIP.2002.1040082.X. Wu,
16 A. S. Karar, K. Zhong, A. P. T. Lau, and C. Lu, "Experimental demonstration of pre-electronic dispersion compensation in IM/DD systems using an iterative algorithm," Opt. Express **29**, 24735-24749 (2021).
17. S. Hu, J. Zhang, J. Tang, W. Jin, R. Giddings, and K. Qiu, "Data-Aided Iterative Algorithms for Linearizing IM/DD Optical Transmission Systems," J. Lightwave Technol. **39**, 2864-2872 (2021).
18. C.-C. Wei, "Analysis and iterative equalization of transient and adiabatic chirp effects in DML-based OFDM transmission systems," Opt. Express **20**, 25774-25789 (2012).